RSC Advances

PAPER

View Article Online
View Journal | View Issue

Cite this: *RSC Adv.*, 2024, **14**, 36610

Synthesis of highly activated polybenzene-grafted carbon nanoparticles for supercapacitors assisted by solution plasma

Quoc Phu Phan, *[ab] Thi Cam Linh Tran,[ab] Thanh Tung Tran,[ab] Thi Thai Ha La,[ab] Xuan Viet Cao,[ab] Tuan Anh Luu[bc] and Thi Quynh Anh Luong[bd]

The growing demand for electronic storage devices with faster charging rates, higher energy capacities, and longer cycle lives has led to significant advancements in supercapacitor technology. These devices typically utilize high-surface-area carbon-based materials as electrodes, which provide excellent power densities and cycling stability. However, challenges such as inadequate electrolyte interaction, hydrophobicity that impedes ion transport, and high manufacturing costs restrict their effectiveness. This study aims to enhance carbon-based materials by grafting polymer chains onto their surfaces for supercapacitor applications. A simple solution plasma process (SPP), followed by heating, prepared the polymer-grafted carbon materials. Carbon nanoparticles were synthesized from benzene through plasma discharge in liquid under ambient conditions, forming free radical sites on the carbon surface. Subsequently, benzene molecules were grafted onto the surface *via* radical polymerization during heating. We investigated the structural and morphological properties of the synthesized materials using scanning electron microscopy (SEM), transmission electron microscopy (TEM), Fourier transform infrared spectroscopy (FTIR), X-ray powder diffraction (XRD), and Raman spectroscopy. Additionally, N_2 absorption–desorption isotherms were measured, pore structure was analyzed with the Dubinin–Astakhov (DA) average pore size model, and specific surface area was determined using the Brunauer–Emmett–Teller (BET) equation for all synthesized samples. The results indicated that the grafting process was influenced by heating time and drying temperature. Furthermore, the electrical properties of the samples were evaluated using cyclic voltammetry (CV), which demonstrated enhancements in both areal capacitance and cycling stability for the polybenzene-grafted carbon compared to the non-grafted variant. This research illustrates that polymer grafting can effectively improve the performance and stability of carbon-based materials for supercapacitor applications. Future work will aim to optimize these materials for broader applications.

Received 10th September 2024
Accepted 11th November 2024

DOI: 10.1039/d4ra06534d

rsc.li/rsc-advances

Introduction

The current century has witnessed an immediate surge in energy demand due to rapid technological advancements, transportation expansion, and population growth. Traditionally, energy requirements have primarily been fulfilled through fossil fuels, including coal, oil, and natural gas, which have been the foundation of the global energy supply for decades. However, these resources' environmental impacts and limited availability have created an urgent demand for sustainable alternatives. In response to these challenges, scientists and researchers have concentrated on developing alternative energy sources, such as solar, wind, tidal, geothermal, hydroelectric, and fuel cells.[1] Furthermore, improvements to existing materials and the advancement of new materials have been pursued to enhance efficiency, reduce costs, and improve the applicability of sustainable energy technologies, such as batteries, supercapacitors, fuel cells, and other technologies designed to address long-term challenges.[2] As a popular technological advancement, supercapacitors have emerged as a potential energy storage medium capable of replacing conventional batteries in various applications due to their significant charge storage capacity, fast discharge rates, high specific power, exceptional cycling life, and environmentally sustainable properties.[3,4] The composition of the electrode, separator, and

[a]*Department of Polymer Materials, Faculty of Materials Technology, Ho Chi Minh City University of Technology (HCMUT), 268 Ly Thuong Kiet Street, District 10, Ho Chi Minh City, Vietnam, Vietnam. E-mail: pqphu@hcmut.edu.vn; linh.trancamlinh12@hcmut.edu.vn; tung.tran.129k19@hcmut.edu.vn; lathaihapolyme@hcmut.edu.vn; caoxuanviet@hcmut.edu.vn*

[b]*Vietnam National University Ho Chi Minh City, Linh Trung Ward, Thu Duc City, Ho Chi Minh City, Vietnam, Vietnam*

[c]*Department of Energy Materials and Applications, Faculty of Materials Technology, Ho Chi Minh City University of Technology (HCMUT), 268 Ly Thuong Kiet Street, District 10, Ho Chi Minh City, Vietnam, Vietnam. E-mail: luutuananh@hcmut.edu.vn*

[d]*Department of Metallurgy and Alloy Materials, Faculty of Materials Technology, Ho Chi Minh City University of Technology (HCMUT), 268 Ly Thuong Kiet Street, District 10, Ho Chi Minh City, Vietnam, Vietnam. E-mail: ltqanh@hcmut.edu.vn*

electrolyte primarily determines the efficiency and feasibility of supercapacitors. As a result, the focus of significant research and innovation in this field has been on developing advanced materials for supercapacitor components.

Carbon-based nanomaterials have been widely selected as essential materials in developing high-performance supercapacitor electrodes within the nanotechnology area. This is due to their unique properties, including good electrical conductivity, high mechanical stability, excellent chemical resistance, and significant surface area and porosity.[5] To enhance the electrochemical performance of supercapacitors, the common goal is to fabricate materials with optimal surface area, conductivity, and electrochemical stability, which can improve energy storage and power transmission capabilities. Larger surface area electrodes have been provided, leading to more active sites for the interaction of ions in the electric double-layer capacitor (EDLC) charge storage mechanisms.[6] As a result, the superior properties and large specific surface area of nanocarbon materials, such as activated carbon, carbon nanotubes, and graphene, have been studied as potential materials for electrode applications. However, due to their small size, typically only a few nanometers, carbon materials are susceptible to aggregation resulting from the direct mutual attraction between nanoparticles through van der Waals forces or chemical bonding.[7] This aggregation limits the electrochemical stability of the nanocarbon materials. Therefore, it is essential to acknowledge the chemical aspects of electrochemical stability, particularly the importance of edge sites. Furthermore, the hydrophobic surfaces with poor interaction abilities of nanocarbon hinder charge transfer efficiencies, and the high cost of modern manufacturing processes limits the application area.[8] To address these challenges, many methods have been developed to modify the carbon properties, such as physical coating, chemical covalent bonding, and non-covalent bonding.[9–11]

The functionalization of carbon materials with polymers has garnered significant attention as a means to enhance the dispersion ability, chemical stability, electrical conductivity, and electrical properties of these materials.[12–14] Considerable progress has been made in material selection, structural design, and surface engineering in this field. The grafting of polymers onto carbon-based nanomaterials is an active area of research, with scientists collaborating to enable practical applications. Researchers have made significant advancements in material selection, structural design, and surface engineering, including the chemical functionalization of carbon surfaces, as investigated by Kumagai *et al.* Additionally, Chen *et al.* developed a method that combines the "grafting to" and "grafting from" approaches.[15,16] Furthermore, new grafting techniques have also been explored, such as Tanaka's work on chemical vapor deposition synthesis[17] and O'Brien *et al.*'s electrochemically mediated atom transfer radical polymerization method.[18] Additionally, the effects of polymer grafting on the dispersibility of carbon have been studied, with Cohen *et al.* enhancing the dispersibility of carbon nanotubes in epoxy resin [19]. Moreover, research has focused on the large-scale applications of polymer-grafted carbon-based nanomaterials, as exemplified by Hata's work on carbon materials for thermal energy applications.[20] However, the current techniques of surface oxidation using strong acids result in limited polymer graft density, and the high-technology and extreme reaction conditions required for fabrication are concerns. Furthermore, the bonding between the polymer and carbon is based on functional group reactions, which can lead to low chemical resistance and durability of the resulting materials. The mentioned significant limitations are in terms of polymer graft density, reaction conditions, and the strength of the polymer–carbon bond. These limitations highlight the need for more efficient and durable methods to advance and practically implement these innovative materials.

In this context, the solution plasma process (SPP) has emerged as a recent development, attracting the interest of researchers as a new method for synthesizing carbon nanoparticles and for other applications such as surface modification, sterilization procedures, or toxic compound decomposition.[21] Solution plasma is a non-equilibrium plasma characterized by the movement of electrons and ions due to the plasma discharge in a liquid solution upon applying a high voltage between two submerged electrodes. Recent studies have demonstrated the effective use of plasma solutions in producing various nanomaterials, including carbon allotropes,[22–24] carbon–metal core–shells,[25–27] and carbon–carbon complexes.[28–30] During the solution plasma process (SPP), the precursor molecules are excited, and the molecules around the electrode are bombarded by the released electrons, forming highly reactive species, such as ions, electrons, radicals, and photons. These activated particles prompt the appropriate chemical reactions to produce nanocarbon with stable quality.[31] Furthermore, the solution plasma method generates more activated chemical species, which can act as initiators for the polymerization process. This offers the potential to overcome the limitations of the current grafting approaches.

Aiming to develop a more effective method for fabricated polymer-grafted carbon material, this research proposes a novel solution plasma processing (SPP) approach followed by a heating process without requiring extra catalysts and chemicals except benzene precursor. The SPP produces carbon material with a high concentration of free radicals on its surface during the plasma discharge at room temperature and atmospheric pressure. Subsequently, the benzene molecules are grafted and polymerized onto the carbon surface *via* the free radical addition process. The key benefit of this synthesis approach is the facile generation of the polybenzene-grafted carbon material. Characterization techniques, such as transmission electron microscopy (TEM), scanning electron microscopy (SEM), Fourier transform infrared spectroscopy (FTIR), X-ray powder diffraction (XRD), and Raman spectroscopy, have confirmed the successful grafting of the polybenzene chains on the carbon surfaces. Furthermore, the cyclic voltammetry (CV) analysis has shown that the electrical properties of the grafted samples are much higher than those of the pure carbon sample. The effects of heating time and drying temperature on the grafting of carbon material were evaluated by varying several experimental parameters.

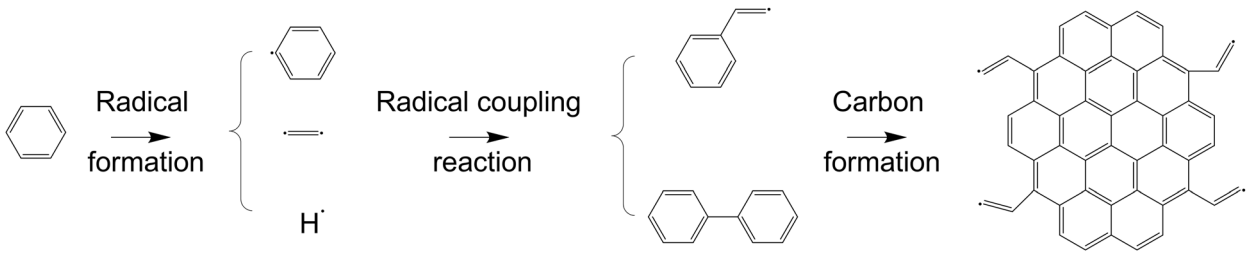

Fig. 1 Reaction path for the formation of carbon products during the solution plasma process.

Experimental procedure

Synthesis of carbon material

In this experimental setup, 50 ml of benzene (C_6H_6, 99.5% purity, China) solvent was poured into a glass reactor and magnetically stirred at 100 rpm. Two 1.0 mm diameter tungsten electrodes (W, 99.0% purity, China) wrapped in insulated PVC tubing were placed into the glass reactor, with their tips submerged in the benzene solution and a gap distance of 1.0 mm between them. Plasma was generated between the tungsten electrode tips using a Vinasemi 305D DC power supply with a high-voltage generator ignition module. The electrical power and voltage of the plasma were set to 10 W and 2.0 kV, respectively. The benzene solvent was decomposed into free radicals during the plasma discharge at room temperature and standard atmospheric pressure, producing carbon materials (Fig. 1). The decomposition of the benzene solvent and the subsequent generation of the carbon material have occurred through the action of the high-energy plasma discharge.[31–34]

Following the 30 minutes plasma discharge, the carbon product was separated and washed using a vacuum filtration device with a 0.22 μm pore size nylon filter and acetone solvent. The collected carbon powder was then dried in an oven at 200 °C for one hour. The fabricated product, named the S-30 sample, was stored in a brown bottle at room temperature. A schematic diagram of the synthesis process for the S-30 sample was presented on Fig. 2.

Synthesis of polybenzene-grafted carbon material

Polybenzene-grafted carbon compounds were synthesized in two distinct stages, as illustrated in Fig. 2. The initial step involved the creation of carbon materials using the SPP method. After 30 minutes of plasma discharge in the liquid phase, the resulting carbon solution was heated to 80 °C using a hot water bath. During the heating process, the free radical sites on the carbon surfaces facilitated the transfer of these reactive species to the benzene molecules, forming cyclohexadienyl radicals on

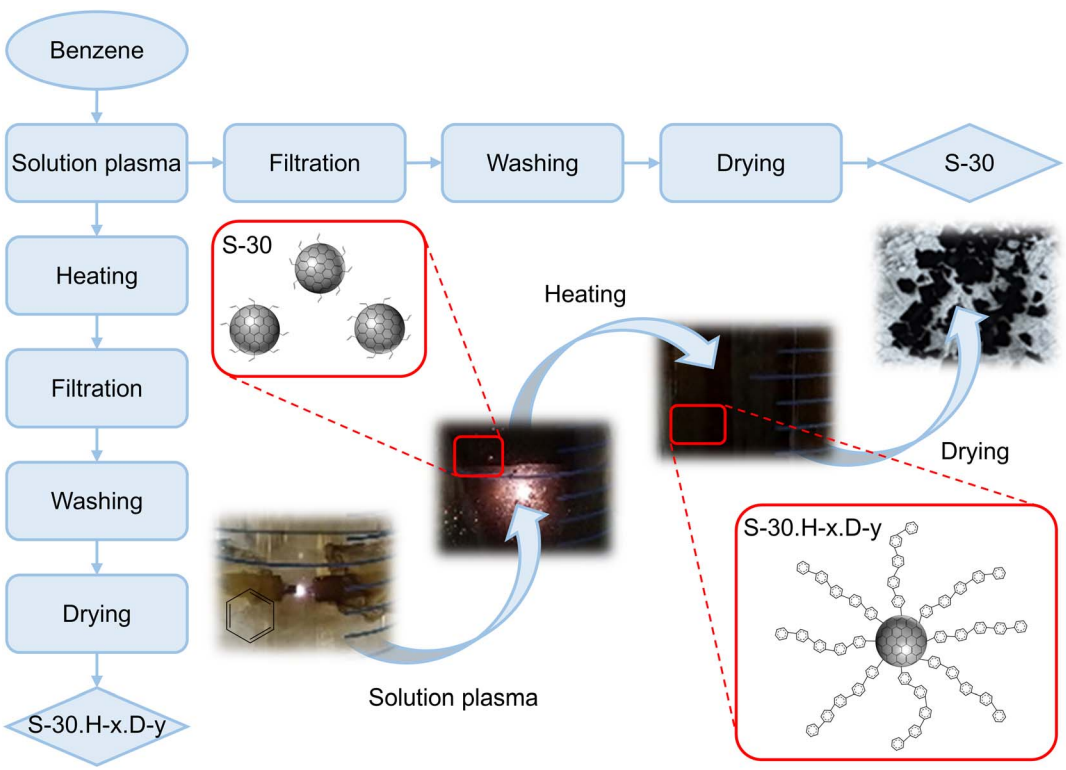

Fig. 2 Schematic diagram of the preparation process of S-30 and S-30.H-*x*.D-*y* samples.

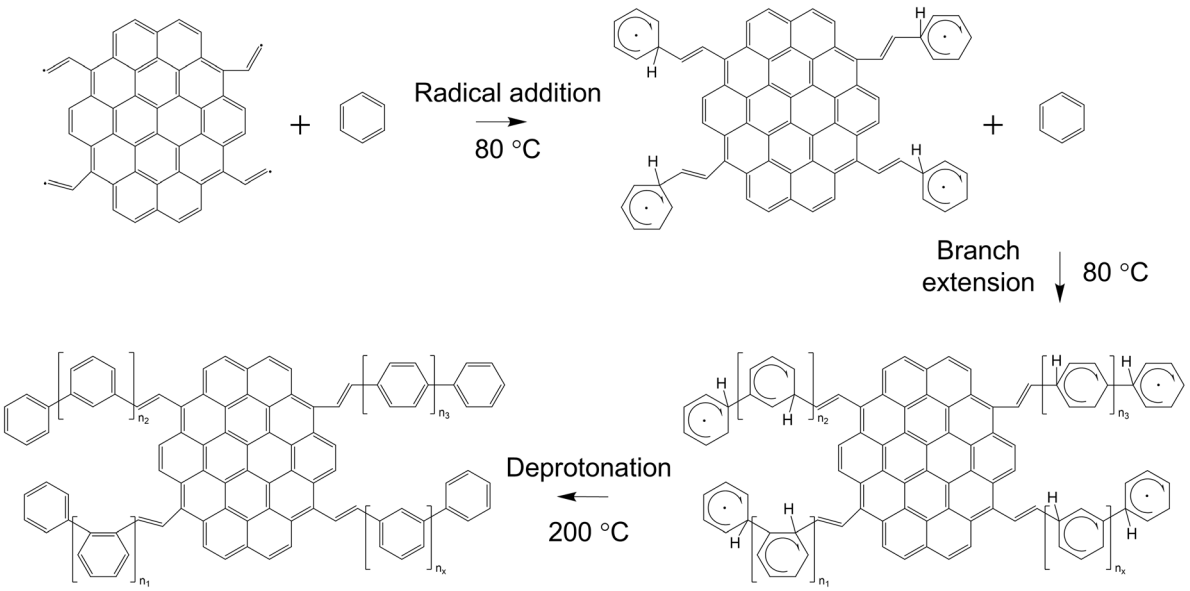

Fig. 3 Reaction path for the formation of polybenzene-grafted carbon products during the heating process.

the carbon surfaces.[35,36] The free radicals on the cyclohexadienyls were further activated and subsequently reacted with additional benzene molecules, leading to the growth and grafting of polybenzene chains onto the carbon surface.[37] The reaction pathway for forming the polybenzene-grafted carbon materials is depicted in Fig. 3. Combining the solution plasma technique and the heating-induced radical polymerization, this two-stage approach enabled the synthesis of the polybenzene-grafted carbon compounds.

To investigate the impact of the heating process on the growth of the polybenzene chains, the reaction time was varied from 3 to 6 hours at ambient temperature and normal atmospheric pressure. After the heating step, the synthesized samples were separated and washed using the previously described procedure. The obtained carbon powder was then dried in an oven for 1 hour. During the drying, the hydrogen atoms on the cyclohexadienyl rings were eliminated through the deprotonation process.[36] The effect of the drying process on the deprotonation was also considered by changing the drying temperature from 100 °C to 200 °C. The synthesized products were named using the convention S-30.H-*x*.D-*y*, where 'S-30' refers to the solution plasma process duration of 30 minutes, 'H-*x*' denotes the heating time in hours, and 'D-*y*' indicates the drying temperature in celsius degrees. The final products were stored in brown bottles at room temperature. This systematic approach, investigating both heating time and drying temperature, provided insights into optimizing the polybenzene chain growth and the deprotonation process during the synthesis of carbon-based materials.

Material characterisation

The synthesized sample powders were utilized for all measurements to assess the morphological and structural characteristics. The surface characteristics of the carbon samples under different synthesis conditions were analyzed by a scanning electron microscope (SEM) method using an S-4800 FE-SEM device made in Japan. The morphologies and structures of the synthesized samples were determined by a transmission electron microscope (TEM) using a JEOL-2100 TEM made in Japan with an operated accelerating voltage of 200 kV. Fourier-transform infrared spectroscopy (FTIR) was employed with wavenumbers ranging from 500 cm^{-1} to 4000 cm^{-1} to identify functional groups in the samples using a Thermo Nicolet 6700 FT-IR Spectrometer made in the United States. X-ray diffraction (XRD) was utilized to measure the crystallinity of the samples using a Malvern Panalytical B.V. system made in Netherlands with CuKα radiation (λ = 0.154 nm). The crystallinities and structures of the synthesized samples were further examined by Raman spectroscopy using an XploRA ONE™ Raman Microscope instrument made in Japan with wavenumbers ranging from 500 cm^{-1} to 3000 cm^{-1}. The N_2 adsorption–desorption isotherms of the samples at liquid nitrogen temperature (78 K) and within the gas saturation vapor tension range were measured using a Nova e-4000 device manufactured in the United States, while the surface areas, porosity, and pore size distributions were estimated employing Brunauer–Emmett–Teller (BET) isotherms, Barrett–Joyner–Halenda (BJH) method, and Dubinin–Astakhov (DA) model.

Cyclic voltammetry (CV) measurements were conducted using three-electrode cells with a Bio-Logic MPG2 potentiostat (manufactured in France) to assess the electrochemical properties of the synthesized samples. The configuration of the three-electrode system included a glassy carbon disk with a diameter of 3 mm, designated as the working electrode; a platinum electrode serving as the counter electrode; and a silver/silver chloride (Ag/AgCl) electrode functioning as the reference electrode. The CV measurements were performed on a mixture comprising 70% synthesized sample, 15% carbon C65, and 15% carboxymethyl cellulose (CMC) binder, all dispersed in a 0.5 N H_2SO_4 solution. The measurements were

carried out at a scan rate of 50 mV s^{-1} over a potential range of 0.0 to 1.4 V *vs.* RHE (reversible hydrogen electrode) at room temperature and typical atmospheric pressure.

Results and discussions

Scanning electron microscope (SEM) measurements

The surface structures of the pure carbon and the grafted carbon samples obtained under different synthesis conditions were analyzed using SEM, and the results are presented in Fig. 4. The SEM images of the S-30 sample, shown in Fig. 4a and b, exhibit a rough surface due to the aggregation of carbon particles. Before the grafting modification, the fabricated carbon particles appear as spherical entities with distinct particle boundaries. Compared to the original carbon samples, the grafted samples display smoother surfaces, indicating that the polymer chains have been successfully grafted onto the carbon surfaces.[38] This observation suggests that the grafting process has effectively modified the surface characteristics of the carbon materials. Furthermore, the SEM images of the S-30.H-6.D-200 sample exhibit continuous surfaces, which implies that the extended heating time of 6 hours has significantly influenced the grafting process of the polybenzene chains onto the carbon surfaces. These SEM findings provide visual evidence of the surface morphological changes that occur during the grafting process, highlighting the impact of the synthesis conditions, particularly the heating time, on the formation and distribution of the polybenzene chains on the carbon surfaces.

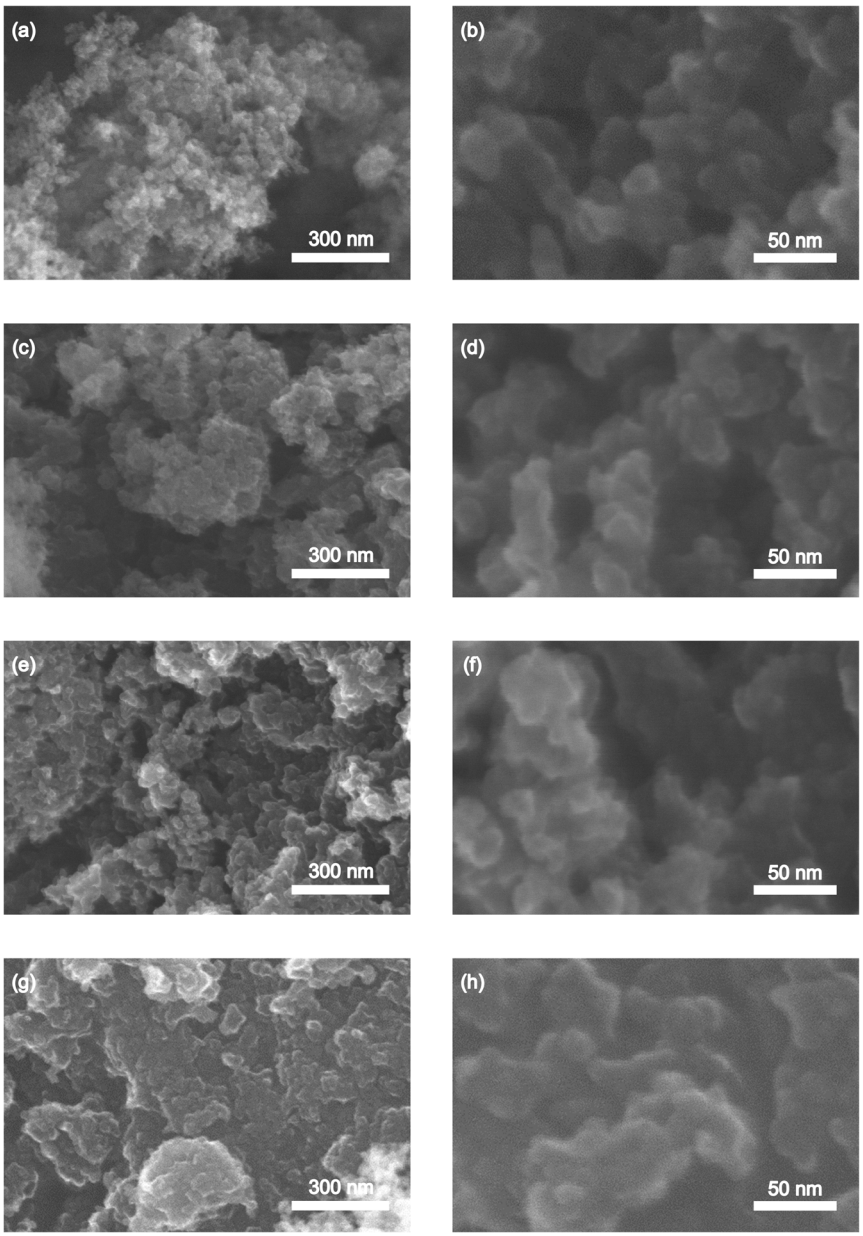

Fig. 4 SEM images of the surface of the synthesized samples: S-30 (a and b), S-30.H-3.D-100 (c and d), S-30.H-3.D-200 (e and f), and S-30.H-6.D-200 (g and h).

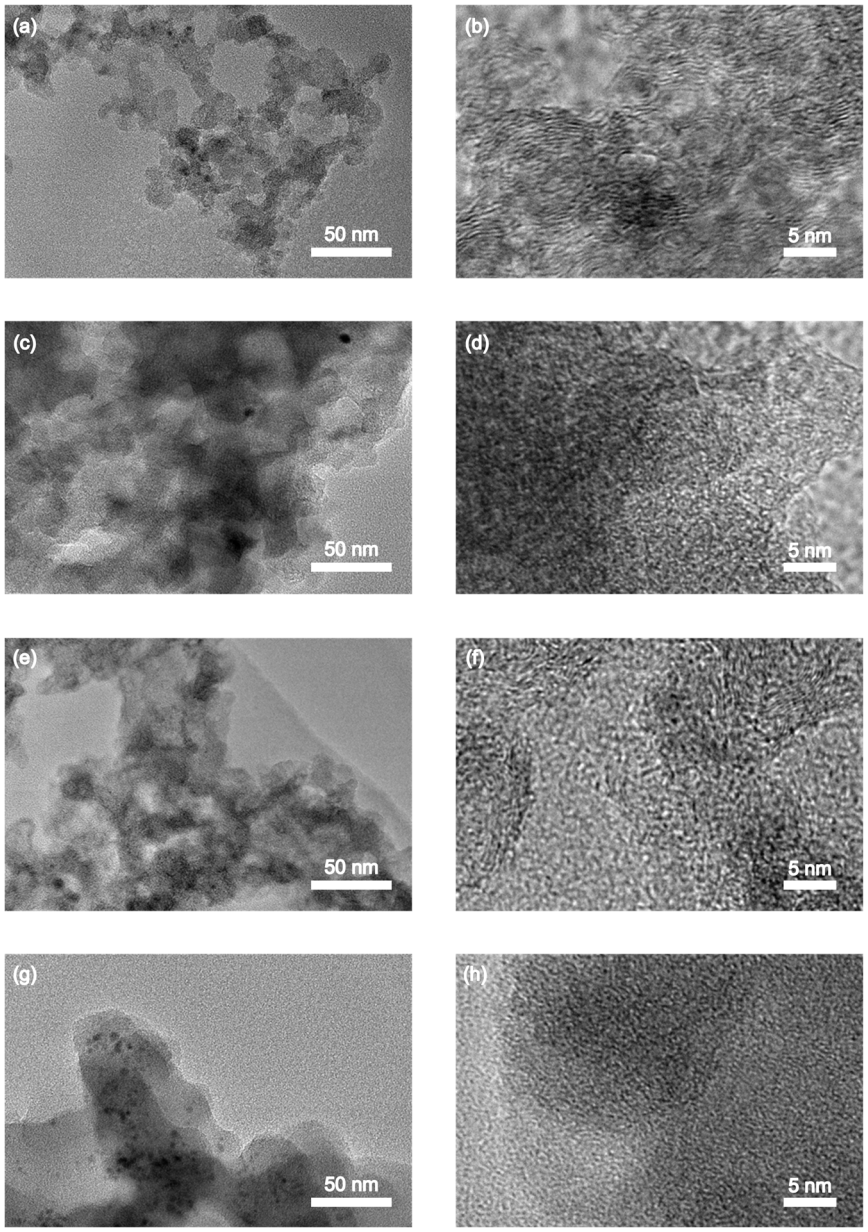

Fig. 5 TEM images of the surface of the synthesized samples: S-30 (a and b), S-30.H-3.D-100 (c and d), S-30.H-3.D-200 (e and f), and S-30.H-6.D-200 (g and h).

Transmission electron microscopy (TEM) measurements

Transmission electron microscopy (TEM) is a widely used technique to analyze the morphology of materials. As the low-magnification TEM image in Fig. 5a reveals that the S-30 sample exhibits a chain-like structure composed of uniform-sized carbon particles formed by aggregating primary carbon particles. Interestingly, the TEM micrographs of the grafted carbon samples show an increase in the size of the carbon particles and the formation of larger aggregation clusters. This observation indicates that the polybenzene chains have been successfully grafted onto the carbon surface using the proposed method. At higher magnification (Fig. 5b), the TEM images of the S-30 sample reveal the crystal lattices of graphitized carbon parts, where the carbon layers are arranged in a parallel pattern.[39] In contrast, the TEM images of the grafted samples with 3 hours of heating show a less distinct parallel pattern, suggesting the influence of the grafted polybenzene chains. Furthermore, the TEM image of the S-30.H-6.D-200 sample, which underwent extended heating of 6 hours, exhibits no clear parallel pattern due to the extensive coverage of the carbon surface by the polybenzene chains. These TEM findings provide structural insights into the impact of the grafting process on the morphology and crystallinity of the carbon materials, highlighting the changes in the particle size, aggregation, and the disruption of the parallel carbon layer arrangement as a result of the successful grafting of the polybenzene chains.

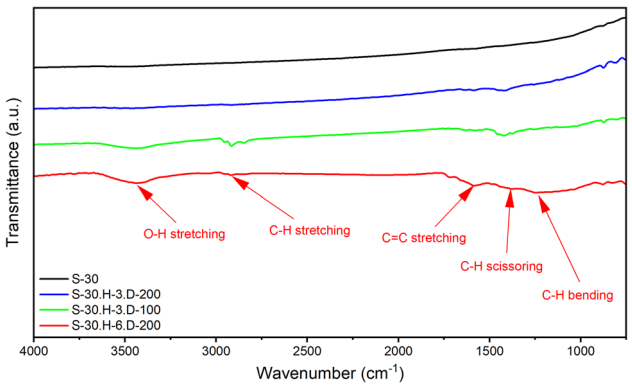

Fig. 6 FTIR spectra of the S-30, S-30.H-3.D-100, S-30.H-3.D-200, and S-30.H-6.D-200 samples.

Fourier-transform infrared spectroscopy (FTIR) measurements

Fourier-transform infrared spectroscopy (FTIR) is a crucial analytical technique to detect structural changes in synthesized samples. As shown in Fig. 6, all the grafted carbon samples exhibit the presence of the benzene ring plane, as evidenced by the scissoring and stretching vibrations of C–H at 1390 cm^{-1} and C=C at 1590 cm^{-1}, respectively.[40–42] In contrast, these characteristic vibrations were absent in the FTIR spectrum of the S-30 sample, indicating the lack of polybenzene chains on its surface. This observation confirms that the polybenzene chains have been successfully grafted onto the carbon surface using the proposed method. Further analysis of the FTIR spectra reveals additional insights. The FTIR spectrum of the S-30.H-3.D-100 sample shows a band at 2900 cm^{-1}, corresponding to the C–H stretching vibrations of the hydrogen bonds on the cyclohexadienyl rings.[43] However, this C–H stretching vibration is no longer present in the spectrum of the S-30.H-3.D-200 sample, suggesting that the deprotonation process was completed during the drying stage at 200 °C. Additionally, the FTIR spectra of the S-30.H-3.D-100 and S-30.H-6.D-200 samples exhibit additional bands at 3450 cm^{-1}, which can be attributed to moisture adsorption.[44] This observation indicates that the hydrophobic nature of the carbon material has been affected by the grafting of the polybenzene chains. Overall, the FTIR spectroscopy analysis provides clear evidence of the successful grafting of the polybenzene chains onto the carbon surface and the associated structural changes, including the presence of the benzene ring, the completion of the deprotonation process, and the altered hydrophobic properties of the carbon material.

X-ray diffraction analysis (XRD) measurements

X-ray diffraction (XRD) analysis was used to examine the diffraction patterns of the fabricated samples. As shown in Fig. 7a, all the samples exhibit a similar peak at 25°, which can be attributed to the diffraction of carbon in the XRD patterns.[31,45] The broad nature of these bands indicates that the structures of the fabricated samples are predominantly amorphous. Additionally, all the samples displayed the presence of tungsten complexes in their XRD patterns. Specifically, the peaks at 39° corresponding to WO were observed in all the synthesized samples, suggesting that an oxidation process occurred during the drying process in the oven.[46] However, the intensity of the WO peak at 39° in the pure carbon sample was noticeably more substantial than in the grafted samples. This observation indicates that the fabricated polybenzene chains partially protected the tungsten particles in the grafted samples. Furthermore, the XRD patterns also reveal another series of diffraction peaks of lower intensity at different 2θ positions, which can be attributed to WC and WC_{1-x}.[47] These XRD findings provide structural insights into the fabricated samples, highlighting the amorphous nature of the carbon structures and the presence of tungsten complexes.

Raman spectroscopy measurements

Raman spectroscopy was employed as a fast and non-destructive method to characterize the structure of the

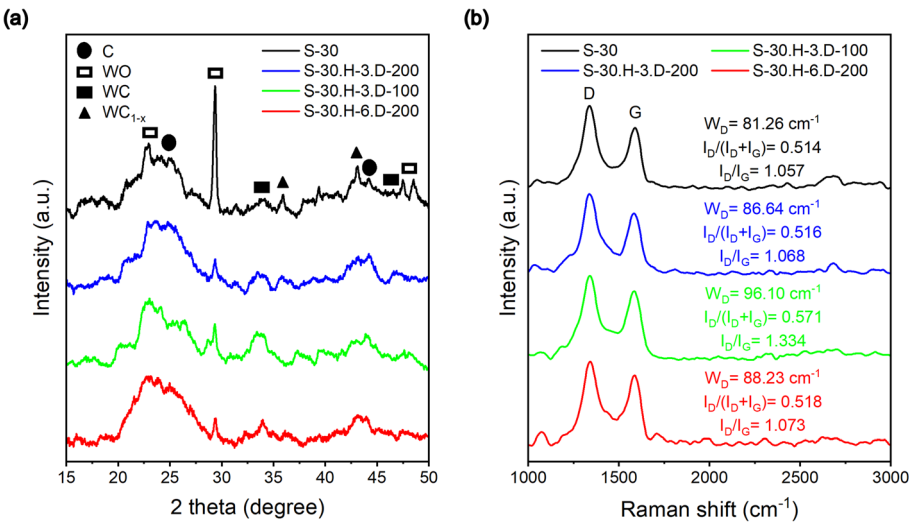

Fig. 7 XRD of the S-30, S-30.H-3.D-100, S-30.H-3.D-200, and S-30.H-6.D-200 samples.

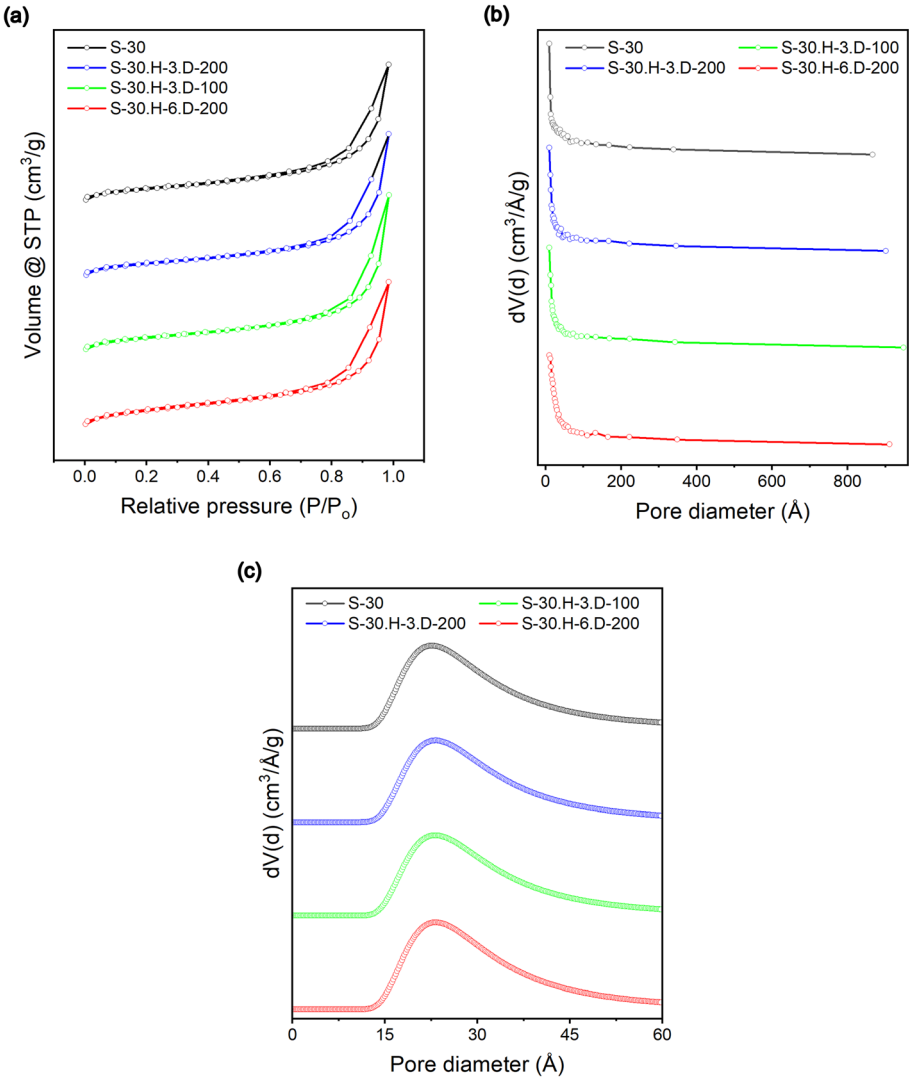

Fig. 8 Specific surface area (a), BJH pore radius (b), and DA average pore size (c) of the S-30, S-30.H-3.D-100, S-30.H-3.D-200, and S-30.H-6.D-200 samples.

generated carbon materials. As shown in Fig. 7b, the Raman spectra of all the synthesized samples exhibit the characteristic disordered D band at 1340 cm^{-1} and the graphitic G band at 1580 cm^{-1}.[32] The D band originates from the sp^2 hybridized carbon structure and is associated with dislocations in the plane of the graphitic structure. The G band, on the other hand, corresponds to the vibrations of neighboring atoms moving in opposite directions perpendicular to the plane of the graphitic sheet. These two bands' intensity ratio (I_D/I_G) can be utilized to assess the degree of disorder in the carbon materials. The S-30.H-3.D-100 sample showed the highest I_D/I_G ratio of 1.334, suggesting a high degree of disorder in the synthesized samples. However, the S-30.H-3.D-200 sample significantly reduced the I_D/I_G ratio, bringing it closer to the value observed for the pure carbon sample. Furthermore, the I_D/I_G and the width of the D band (W_D) of the S-30.H-3.D-200 and S-30.H-6.D-200 samples present almost entirely unchanged compared with the non-grafted carbon, indicating that the grafting process only slightly impacted the carbon structure.[48] Overall, the slight increase in the D band intensity observed in the grafted samples may suggest various structural modifications introduced during the grafting process.

BET-specific surface area measurements

BET-specific surface area measurements were performed to quantitatively evaluate the surface characteristics of the carbon materials produced in this research. Fig. 8 illustrates the N_2 adsorption/desorption isotherms and pore size distribution of ungrafted and polybenzene-grafted carbon samples, providing insights into their surface properties. The isotherms, classified as type IV according to IUPAC standards, exhibit a type H3 hysteresis loop between 0.0 and 1.0 (P/P_0), indicative of capillary condensation in the mesoporous structure, characterized by asymmetrical pores and notable interparticle porosity.[49] The pore size distribution, shown in Fig. 8b, was determined using the Barrett–Joyner–Halenda (BJH) method. In contrast, the Dubinin–Astakhov (DA) method was employed to assess average pore sizes based on adsorption and desorption points, as

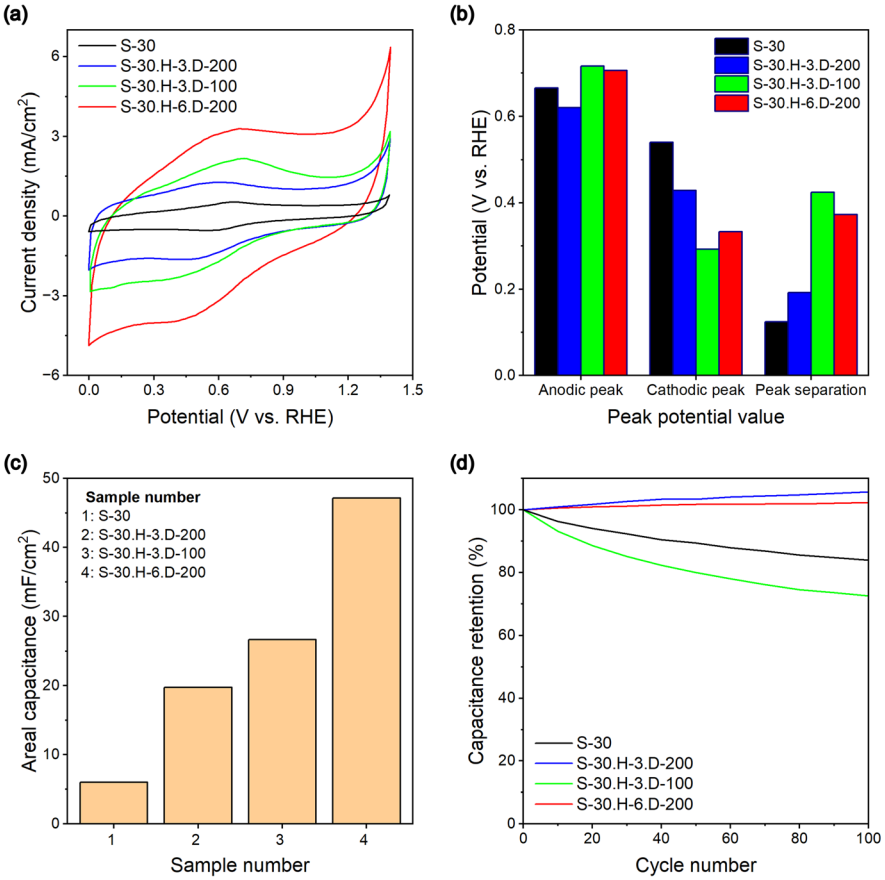

Fig. 9 Cyclic voltammograms (a), peak potential (b), area capacitance (c), and capacitance retention (d) of the fabricated samples at a 50 mV s^{-1} scan rate in 0.5 N H_2SO_4 electrolyte.

depicted in Fig. 8c. Surface area measurements revealed that the BET surface area of the S-30 sample slightly decreased compared to the S-30.H-3.D-100 and S-30.H-3.D-200 samples, with values of 181.470 m^2 g^{-1}, 177.689 m^2 g^{-1}, and 179.417 m^2 g^{-1}, respectively. Conversely, the S-30.H-6.D-200 sample exhibited an increase to 200.222 m^2 g^{-1}. Besides that, the pore diameter measurements remained stable, with peak values around 23 Å, suggesting that polybenzene chains have minimal impacts on the carbon nanoparticles' surface area and the pore size.

Cyclic voltammetry (CV) measurements

Cyclic voltammetry (CV) measurements were conducted to evaluate the electrochemical performance of the samples. The measurements were carried out in a 0.5 N aqueous H_2SO_4 electrolyte at a scan rate of 50 mV s^{-1} within a range from 0.0 to 1.4 V *vs.* RHE potential window, as shown in Fig. 9a. The results demonstrate that the grafted carbon sample's current densities were significantly better than the pure carbon benchmark. Besides that, the calculated areal capacitance of the grafted samples also indicates better values than the original carbon (Fig. 9c). To explain the CV results of the S-30 sample in detail, the electron storage mechanism involves the formation of an electric double-layer capacitor (EDLC) due to the adsorption and desorption of hydrogen ions during the measurement. The researchers propose that positive proton–π binding pairs are formed on the carbon interfaces due to the attraction of the negatively charged surfaces formed by the hexagonal carbon ring.[50,51] During the proton–π binding pair formation, the carbon surfaces repel the positively charged sites on the hexagonal carbon ring (Fig. 10). Each proton–π pair is a positively charged site, and an electron is required to avoid strongly repulsive electrostatic interactions. Hence, the carbon surface must contain more electrons to neutralize most proton–π binding pairs. In the case of the grafted carbon samples, the charge storage mechanisms occurred on the carbon surfaces and the polybenzene chains. For the reactions on the polybenzene branches, the mentioned proton–π binding pairs are also expected to occur within the benzene monomers in the polymer chains.[52] The researchers propose that the increased current density in the CV results of the grafted carbon samples is caused by the effect of the proton–π binding pairs in the polybenzene chains. Due to the measurement, the benzene monomers in the polymer chains produce negatively charged zones, forming the proton–π binding pairs. As a result, the total number of favorable cation interaction sites is increased, leading to a corresponding increase in the electron storage ability of the grafted sample (Fig. 10). Overall, the researchers

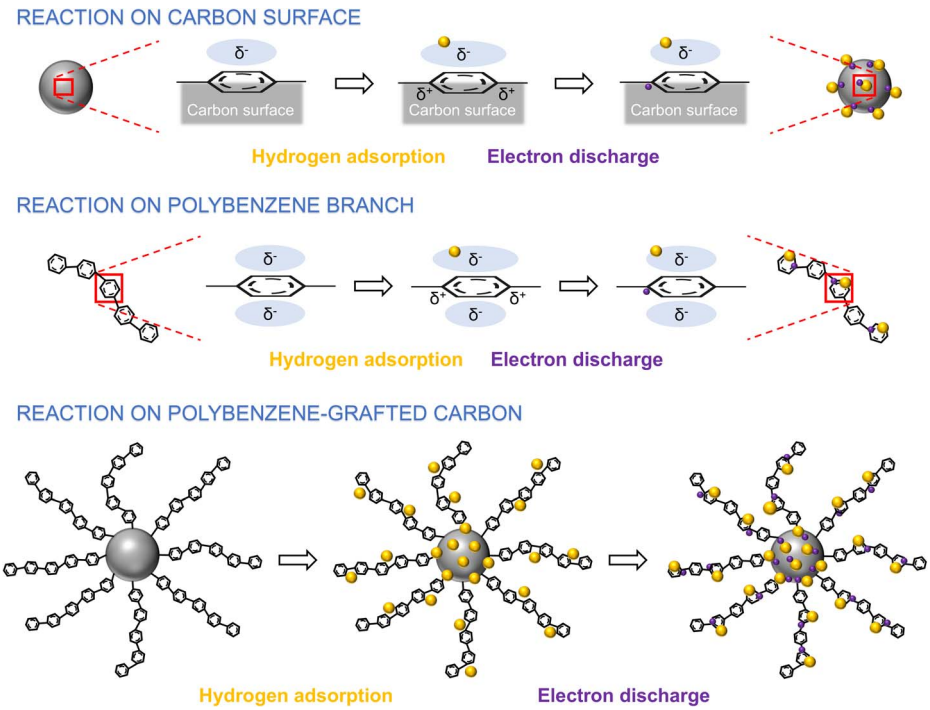

Fig. 10 Schematic illustration of the preparation process for the carbon and polybenzene-grafted carbon samples.

demonstrate that including aromatic-ring groups in polybenzene chains within the grafted carbon provides a strategy for enhancing electron storage performance. The cyclic voltammetry (CV) measurements yielded significant insights into the redox mechanism of hydroquinone. The analysis revealed distinct oxidation and reduction peaks at approximately 0.6 V and 0.4 V *vs.* RHE. These peaks represent the electron transfer processes involved in the oxidation of hydroquinone to benzoquinone and the subsequent reduction back to hydroquinone.[53] Based on the collected redox peak potentials, the carbon-based materials' peak separation (ΔE_p) was calculated to provide insights into their electron characteristic properties. As shown in Fig. 9b, the grafted carbon sample exhibited higher peak separation values in the cyclic voltammetry compared to the pure carbon. A high peak separation indicates an irreversible electrochemical reaction at the carbon electrode–electrolyte interface. This suggests that the electron transfer kinetics at the interface are sluggish, meaning the redox reaction is not readily reversible due to the effect of the polybenzene chains. This result suggests an improvement in the durability of the carbon electrode during the CV measurement. The increased peak separation values in the grafted carbon samples indicate a less reversible redox reaction, which can contribute to the enhanced durability of the electrode material compared to pure carbon.

In this scientific report, the authors also investigated the cycling stability of supercapacitor electrodes synthesized with various modifications. The electrodes were subjected to continuous cyclic voltammetry (CV) cycling for up to 100 cycles at a scan rate of 50 mV s^{-1} in a 0.5 N H_2SO_4 aqueous electrolyte at room temperature to evaluate the cycling stability. The data presented in Fig. 9d shows that the electrodes with the polybenzene chains grafted onto the carbon surfaces, namely S-30.H-3.D-200 and S-30.H-6.D-200, exhibited stable capacitance retention over 100 cycles. In contrast, the S-30 electrode, without the polybenzene functionalization, displayed a decrease in capacitance after 100 cycles. The improved cycling stability of the polybenzene-grafted carbon electrodes can be attributed to the enhanced durability and longevity of the electrode materials. The polybenzene functionalization likely stabilizes the carbon surface, preventing the dissolution of carbon into the aqueous electrolyte, which is the primary cause of the capacitance loss over cycling. Interestingly, the S-30.H-3.D-100 samples showed a dramatic reduction in retention capacity, which might be the effect of hydrogen extraction from the cyclohexadienyl rings due to the CV measurement. In conclusion, the results demonstrate that polybenzene functionalization enhances the durability and longevity of carbon electrodes, making them promising candidates for effective electrode materials in supercapacitor applications.

Conclusions

In this study, the preparation of pure and polymer-grafted carbon materials was successfully achieved using a solution plasma process. The influences of heating time and drying temperature on the properties of the polybenzene-grafted carbon samples were analyzed and compared to the pure synthesized carbon. The results demonstrate that the polybenzene chains grafted onto the carbon surface can be controlled by adjusting the heating time and drying temperature. The polybenzene-grafted carbon materials exhibited enhanced electrical properties compared to the ungrafted

carbon sample. The area capacitances of the grafted carbon materials were superior to that of the pure carbon sample. Moreover, the area capacitance and retention increased with the heating time and drying temperature. These findings suggest that the polybenzene-grafted carbon materials are highly suitable for supercapacitor applications. Furthermore, the ability to control the grafting through the manipulation of processing parameters highlights the versatility of this approach for developing advanced carbon-based materials for energy storage and conversion applications.

Data availability

All data that supports the findings of this study are available from the corresponding author upon reasonable request. This includes the crucial experimental data for the synthesis and characterization of the compounds, as well as the raw data for the electrochemical measurements. Additionally, the computational methods and parameters used in this study, along with the input files and output data, are fully described and available.

Author contributions

Phan Quoc developed the theory and wrote the manuscript. Tran Thi Cam Linh carried out the experiments. Tran Thanh Tung processed the measurement. Cao Xuan Viet contributed to sample preparation. Luu Tuan Anh analyzed the SEM and TEM data. La Thi Thai Ha analyzed the Raman, FTIR, and XRD data. Luong Thi Quynh Anh analyzed the CV data.

Conflicts of interest

There are no conflicts to declare.

Acknowledgements

The Murata Science Foundation funds this research under grant number 23VH08. We acknowledge Ho Chi Minh City University of Technology (HCMUT) and VNU-HCM for supporting this study.

References

1 K. K. Jaiswal, *et al.*, Renewable and sustainable clean energy development and impact on social, economic, and environmental health, *Energy Nexus*, 2022, **7**, 100118.
2 S. Maddukuri, *et al.*, On the challenge of large energy storage by electrochemical devices, *Electrochim. Acta*, 2020, **354**, 136771.
3 P. Sharma and V. J. Kumar, Current technology of supercapacitors: A review, *J. Electron. Mater.*, 2020, **49**(6), 3520–3532.
4 L. Miao, *et al.*, Recent advances in carbon-based supercapacitors, *Mater. Adv.*, 2020, **1**(5), 945–966.
5 J. Xiao, *et al.*, Dimensionality, function and performance of carbon materials in energy storage devices, *Adv. Energy Mater.*, 2022, **12**(4), 2100775.
6 Y. Jiang, *et al.*, Large-surface-area activated carbon with high density by electrostatic densification for supercapacitor electrodes, *Carbon*, 2021, **175**, 281–288.
7 P. Xie, *et al.*, Advanced carbon nanomaterials for state-of-the-art flexible supercapacitors, *Energy Storage Mater.*, 2021, **36**, 56–76.
8 H. Wang, *et al.*, Polymer-derived heteroatom-doped porous carbon materials, *Chem. Rev.*, 2020, **120**(17), 9363–9419.
9 C. Gao, *et al.*, Surface modification methods and mechanisms in carbon nanotubes dispersion, *Carbon*, 2023, **212**, 118133.
10 S. Huang, *et al.*, An overview of dynamic covalent bonds in polymer material and their applications, *Eur. Polym. J.*, 2020, **141**, 110094.
11 A. A. Javidparvar, *et al.*, Non-covalently surface modification of graphene oxide nanosheets and its role in the enhancement of the epoxy-based coatingsphysical properties, *Colloids Surf., A*, 2020, **602**, 125061.
12 P. Eskandari, *et al.*, Polymer-functionalization of carbon nanotube by *in situ* conventional and controlled radical polymerizations, *Adv. Colloid Interface Sci.*, 2021, **294**, 102471.
13 P. Eskandari, *et al.*, Polymer grafting on graphene layers by controlled radical polymerization, *Adv. Colloid Interface Sci.*, 2019, **273**, 102021.
14 H. Randriamahazaka and J. Ghilane, Electrografting and controlled surface functionalization of carbon based surfaces for electroanalysis, *Electroanalysis*, 2016, **28**(1), 13–26.
15 N. Kumagai and M. Shibasaki, Strategic immobilization of molecular catalysts onto carbon nanotubes *via* noncovalent interaction for catalytic organic transformations, *Isr. J. Chem.*, 2017, **57**(3–4), 270–278.
16 J. Chen, *et al.*, A review of the interfacial characteristics of polymer nanocomposites containing carbon nanotubes, *RSC Adv.*, 2018, **8**(49), 28048–28085.
17 K. Tanaka, *et al.*, Effect of carbon nanotube deposition time to the surface of carbon fibres on flexural strength of resistance welded carbon fibre reinforced thermoplastics using carbon nanotube grafted carbon fibre as heating element, *J. Compos. Sci.*, 2019, **3**(1), 9.
18 C. O'Brien and A. Ignaszak, Polymer-grafted-carbon assembled *via* an electrochemically-aided atom transfer radical polymerization: Towards improved energy storage electrode, *Electrochem. Commun.*, 2022, **135**, 107198.
19 S. Cohen, E. Zelikman and R. Y. Suckeveriene, Ultrasonically induced polymerization and polymer grafting in the presence of carbonaceous nanoparticles, *Processes*, 2020, **8**(12), 1680.
20 S. Hata, *et al.*, n-Type carbon nanotube sheets for high in-plane ZT values in double-doped electron-donating graft copolymers containing diphenylhydrazines, *Polym. J.*, 2021, **53**(11), 1281–1286.

21 O. Takai and A. Chemistry, Solution plasma processing (SPP), *Pure Appl. Chem.*, 2008, **80**(9), 2003–2011.
22 S. Chae, *et al.*, -Type doping of graphene with cationic nitrogen, *ACS Appl. Nano Mater.*, 2019, **2**(3), 1350–1355.
23 G. Panomsuwan, C. Chokradjaroen, and N. Saito, Synthesis of nitrogen-doped carbons from single-source precursors by solution plasma, in *Nanomaterials via Single-Source Precursors*, Elsevier, 2022, pp. 475–505.
24 K. Kim, C. Chokradjaroen and N. Saito, Solution plasma: New synthesis method of N-doped carbon dots as ultra-sensitive fluorescence detector for 2, 4, 6-trinitrophenol, *Nano Express*, 2020, **1**(2), 020043.
25 S. Treepet, *et al.*, Solution Plasma Synthesis of Nitrogen-Doped Carbon Dots from Glucosamines: Comparative Fluorescence Modulation for Dopamine Detection, *SSRN Electron. J.*, 2024, **231**, 119705.
26 P. Q. Phan, *et al.*, N-Doped few-layer graphene encapsulated Pt-based bimetallic nanoparticles *via* solution plasma as an efficient oxygen catalyst for the oxygen reduction reaction, *Mater. Adv.*, 2021, **2**(1), 322–335.
27 P. Q. Phan, *et al.*, *In situ* synthesis of copper nanoparticles encapsulated by nitrogen-doped graphene at room temperature *via* solution plasma, *RSC Adv.*, 2020, **10**(60), 36627–36635.
28 K. Sasaki, *et al.*, Solution-Plasma Synthesis and Characterization of Transition Metals and N-Containing Carbon–Carbon Nanotube Composites, *Materials*, 2024, **17**(2), 320.
29 J. Ukai, *et al.*, Nitrogen-Doped Carbon Nanothin Film as a Buffer Layer between Anodic Graphite and Solid Electrolyte Interphase for Lithium–Ion Batteries, *ACS Omega*, 2024, 24372–24378.
30 S. Chae, *et al.*, Single-walled carbon nanotubes wrapped by cationic nitrogen-doped carbon for electrocatalytic applications, *ACS Appl. Nano Mater.*, 2020, **3**(10), 10183–10189.
31 J. Niu, *et al.*, Plasma–Solution Junction for the Formation of Carbon Material, *Coatings*, 2022, **12**(11), 1607.
32 T. Morishita, *et al.*, Fastest formation routes of nanocarbons in solution plasma processes, *Sci. Rep.*, 2016, **6**(1), 36880.
33 D.-w. Kim, *et al.*, Solution plasma synthesis process of tungsten carbide on N-doped carbon nanocomposite with enhanced catalytic ORR activity and durability, *RSC Adv.*, 2014, **4**(32), 16813–16819.
34 C. Chokradjaroen, *et al.*, Fundamentals of solution plasma for advanced materials synthesis, *Mater. Today Adv.*, 2022, **14**, 100244.
35 S. Zhou, *et al.*, Organic super-electron-donors: initiators in transition metal-free haloarene–arene coupling, *Chem. Sci.*, 2014, **5**(2), 476–482.
36 A. Studer and D. P. Curran, Organocatalysis and C–H Activation Meet Radical-and Electron-Transfer Reactions, *Angew. Chem., Int. Ed.*, 2011, **22**(50), 5018–5022.
37 M. Ghasemi, M. H. Moaiyeri and K. Navi, A new full adder cell for molecular electronics, *Int. J. VLSI Des. Commun. Sys.*, 2011, **2**(4), 1–13.
38 X. Wu, *et al.*, Polystyrene grafted carbon black synthesis *via in situ* solution radical polymerization in ionic liquid, *J. Polym. Res.*, 2013, **20**, 1–7.
39 M. M. Thu, *et al.*, Introducing micropores into carbon nanoparticles synthesized *via* a solution plasma process by thermal treatment and their charge storage properties in supercapacitors, *RSC Adv.*, 2023, **13**(24), 16136–16144.
40 Y. Liu, *et al.*, Efficient adsorption of sulfamethazine onto modified activated carbon: a plausible adsorption mechanism, *Sci. Rep.*, 2017, **7**(1), 12437.
41 J. Manuel, T. Salguero and R. P. Ramasamy, Synthesis and characterization of polyaniline nanofibers as cathode active material for sodium-ion battery, *J. Appl. Electrochem.*, 2019, **49**, 529–537.
42 L. Zhao, *et al.*, Effects of the number of benzene rings on the properties of single-source ZrC-based liquid precursors and nano zirconium carbide powders thereof, *Ceram. Int.*, 2021, **47**(23), 32963–32968.
43 F. Feng, *et al.*, Polyphenylsulfone (PPSU)-based copolymeric membranes: effects of chemical structure and content on gas permeation and separation, *Polymers*, 2021, **13**(16), 2745.
44 K. Suresh Kumar Reddy, *et al.*, KOH-based porous carbon from date palm seed: preparation, characterization, and application to phenol adsorption, *Water Sci. Technol.*, 2014, **70**(10), 1633–1640.
45 K.-S. Yun, *et al.*, Preparation of carbon blacks by liquid phase plasma (LPP) process, *J. Nanosci. Nanotechnol.*, 2013, **13**(11), 7381–7385.
46 T. F. Chala, *et al.*, Highly efficient near infrared photothermal conversion properties of reduced tungsten oxide/polyurethane nanocomposites, *Nanomaterials*, 2017, **7**(7), 191.
47 C. B. Rodella, *et al.*, Physical and chemical studies of tungsten carbide catalysts: effects of Ni promotion and sulphonated carbon, *RSC Adv.*, 2015, **5**(30), 23874–23885.
48 A. Cuesta, *et al.*, Raman microprobe studies on carbon materials, *Carbon*, 1994, **32**(8), 1523–1532.
49 S. Fu, *et al.*, Accurate characterization of full pore size distribution of tight sandstones by low-temperature nitrogen gas adsorption and high-pressure mercury intrusion combination method, *Energy Sci. Eng.*, 2021, **9**(1), 80–100.
50 A. Frontera, D. Quinonero and P. M. Deya, Cation–π and anion–π interactions, *Wiley Interdiscip. Rev.: Comput. Mol. Sci.*, 2011, **1**(3), 440–459.
51 N. Luo, *et al.*, Putting Anion-π Interactions at Work for Catalysis, *Chem.–Eur. J.*, 2022, **28**(3), e202103303.
52 M. A. Gebbie, *et al.*, Tuning underwater adhesion with cation–π interactions, *Nat. Chem.*, 2017, **9**(5), 473–479.
53 C. Singh and A. J. T. Paul, Physisorbed hydroquinone on activated charcoal as a supercapacitor: an application of proton-coupled electron transfer, *J. Phys. Chem. C*, 2015, **119**(21), 11382–11390.